



Repositorio Institucional de la Universidad Autónoma de Madrid

<https://repositorio.uam.es>

Esta es la **versión de autor** del artículo publicado en:

This is an **author produced version** of a paper published in:

PHILOSOPHICAL TRANSACTIONS OF THE ROYAL SOCIETY A:
Mathematical, Physical and Engineering Sciences 376.2114 (2018)

DOI: <http://doi.org/10.1098/rsta.2017.0119>

Copyright: © 2018 The Author (s)

El acceso a la versión del editor puede requerir la suscripción del recurso
Access to the published version may require subscription



Subject Areas:

Cosmology, Particle Physics

Keywords:

Inflation, Higgs, Dilaton, Black Holes

Author for correspondence:

Juan García-Bellido

e-mail: juan.garciabellido@uam.es

Higgs-Dilaton Inflation and Primordial Black Holes from Critical Higgs Inflation

Juan García-Bellido¹

¹Instituto de Física Teórica UAM-CSIC, Universidad
Autónoma de Madrid, Cantoblanco, 28049 Madrid,
Spain

We test the Higgs-Dilaton Inflation model using the latest cosmological data sets, including the Cosmic Microwave Background temperature, polarization and lensing data from the *Planck* satellite (2015), the BICEP and Keck Array experiments, the Type Ia supernovae from the JLA catalog, the Baryon Acoustic Oscillations from CMASS, LOWZ and 6dF, the Weak Lensing data from the CFHTLenS survey and the Matter Power Spectrum measurements from the latest SDSS data release. We find that the values of all cosmological parameters allowed by the Higgs-Dilaton model inflation are well within the *Planck* satellite (2015) constraints. In particular, we determine $w_0 = -1.0001^{+0.0072}_{-0.0074}$, $w_a = 0.00^{+0.15}_{-0.16}$, $n_s = 0.9693^{+0.0083}_{-0.0082}$, $\alpha_s = -0.001^{+0.013}_{-0.014}$ and $r_{0.05} = 0.0025^{+0.0017}_{-0.0016}$ (at 95.5% c.l.). We also place new stringent constraints on the couplings of the Higgs-Dilaton model, $\xi_\chi < 0.00328$ and $\xi_h/\sqrt{\lambda} = 59200^{+30000}_{-20000}$ (at 95.5% c.l.). We find that the HDM is only slightly better than the $w_0 w_a$ CDM model, with $\Delta\chi^2 = \chi^2_{w_0 w_a \text{CDM}} - \chi^2_{\text{HDM}} = 0.18$. Given that the HDI model has two fewer parameters, we find Bayesian evidence favoring the HDM over the $w_0 w_a$ CDM model. We also study the Critical Higgs Inflation model, taking into account the running of both the self-coupling $\lambda(\mu)$ and the non-minimal coupling to gravity $\xi(\mu)$. We find peaks in the curvature power spectrum at scales corresponding to the critical value μ , that reenter during the radiation era and collapse to form a broad distribution of clustered primordial black holes, which could constitute today the main component of Dark Matter.

1. Introduction

Physics has often been successful relating apparently different phenomena into a common, unifying framework. The Higgs-Dilaton Inflation model (HDM) was proposed along those lines in Refs. [1–3]. The model has its roots in the Higgs-Inflation paradigm [4,5], and it is based on a non-minimal extension of the Standard Model (SM) to Unimodular Gravity (UG), a restricted version of General Relativity (GR) in which the metric determinant is fixed to one. Its main motivation is to explain the origin of inflation and the seeds of structure in the universe, as well finding a relation between three very different scales of Physics – the Planck scale M_P , the EW scale via the Higgs's vacuum expectation value v , and a cosmological constant Λ – that appear when non-minimally coupling the SM to UG.

The HDM contains two scalar fields: the SM Higgs h and a new dilaton field χ , both non-minimally coupled to gravity. It is by construction scale-invariant (SI) at the classical level, and all the SM scales originate from the spontaneous breakdown of SI. It can explain inflation as a consequence of the slow-roll of the h and χ fields in the early universe. Also, it provides a source of the dark-energy-driven expansion of the late universe (see Ref. [2]) once the fields reach their approximate ground state and start to roll down their potential valley. Therefore, the HDM bridges these two paradigms and uniquely provides an explanation of the current accelerated expansion of the universe from a common inflationary paradigm.

The connection between the two eras allows to relate inflation observables (namely, the primordial scalar power spectrum index n_s and its running α_s) to those observables associated with dark-energy (the dark-energy equation of state parameter w_{DE}^0 and its evolution w_{DE}^a), as they all depend on the HDM parameters (the coupling constant of the Higgs, ξ_h , and the dilaton, ξ_χ , to gravity, and the Higgs quartic self-coupling λ). Even though the cosmological constant model is very successful in describing the evolution of the Universe [6], it still faces several apparently serious theoretical issues [7], especially regarding to the predictivity and testability of the inflationary paradigm.

In Ref. [8] we tested the viability of the Higgs-Dilaton model by comparing it to the cosmological constant (Λ CDM) and evolving Dark Energy ($w_0 w_a$ CDM) models, by using the latest cosmological data sets, including the Cosmic Microwave Background (CMB) temperature, polarization and lensing data from the *Planck* satellite (2015), the BICEP and Keck Array experiments, the Type Ia supernovae from the JLA catalog, the BAO from CMASS, LOWZ and 6dF, the Weak Lensing data from the CFHTLenS survey and the Matter Power Spectrum measurements from the SDSS (data releases DR9-13). To compare with data we had to implement the necessary modifications to the COSMOMC suite in order to impose constraints on the HDM parameters. By testing the compatibility of the model with present observations, we also provided insight on which future probes may be able to discern the model from the standard cosmological constant model Λ CDM and the evolving Dark Energy ($w_0 w_a$ CDM) model in which is nested.

(a) Non-minimal SM coupling to General Relativity

The simplest models of inflation compatible with Planck (2015) data are those sourced by a single scalar field, and one may be tempted to identify such a field with the only fundamental scalar particle found, the Higgs boson h . Such models, however, are not compatible with electroweak experiments, see Ref. [9]. The next simplest possibility is to introduce a new, massless scalar degree of freedom, hereafter called the dilaton χ . Neglecting the SM contributions, the scale-invariant extension for the SM plus GR including the dilaton is [1]

$$\frac{\mathcal{L}_{\text{SI}}}{\sqrt{-g}} = \frac{1}{2} \left(\xi_\chi \chi^2 + \xi_h h^2 \right) R - \frac{1}{2} \partial^\mu h \partial_\mu h - \frac{1}{2} \partial^\mu \chi \partial_\mu \chi - V(h, \chi), \quad (1.1)$$

where the scalar potential is

$$V(h, \chi) = \frac{\lambda}{4} \left(h^2 - \frac{\alpha}{\lambda} \chi^2 \right)^2 + \beta \chi^4, \quad (1.2)$$

and h is the Higgs field in the Unitary Gauge. Note that for the term multiplying the Ricci curvature in Eq. (1.1) to be positive, the couplings must also be $\xi_\chi, \xi_h \geq 0$.

The classical ground states are

$$h_0^2 = \frac{\alpha}{\lambda} \chi_0^2 + \frac{\xi_h}{\lambda} R, \quad R = \frac{4\beta\lambda}{\lambda\xi_\chi + \alpha\xi_h} \chi_0^2, \quad (1.3)$$

which simplify greatly if $\beta = 0$, a parameter that determines whether space-time is flat ($\beta = 0$), de Sitter ($\beta > 0$) or anti-de Sitter ($\beta < 0$) for a particular scalar curvature R whose sign is controlled by β . Note that the solutions for with $\chi_0 \neq 0$ spontaneously break scale-invariance, and so all induced scales are proportional to χ_0 . In particular, the three SM induced scales are (see Ref. [2])

$$M_P^2 = \left(\xi_\chi + \xi_h \frac{\alpha}{\lambda} + \frac{4\beta\xi_h^2}{\lambda\xi_\chi + \alpha\xi_h} \right) \chi_0^2, \quad (1.4)$$

$$\Lambda = \frac{\beta M_P^4}{(\xi_\chi + \alpha\xi_h/\lambda)^2 + 4\beta\xi_h^2/\lambda}, \quad (1.5)$$

$$m_h^2 = M_P^2 \frac{2\alpha(1 + 6\xi_\chi) + 2\alpha^2(1 + 6\xi_h)/\lambda}{\xi_\chi(1 + 6\xi_\chi) + \xi_h\alpha(1 + 6\xi_h)/\lambda}. \quad (1.6)$$

One may worry how the introduction of a new scalar degree of freedom would alter the SM phenomenology, but, as shown in Ref. [10], the dilaton completely decouples from all Standard Model fields except for the Higgs (to which it is coupled derivatively), through Planck-suppressed terms of order m_h^2/M_P^2 . This means that the dilaton does not alter the low energy SM phenomenology, thus making the HDM a viable effective field-theory extension of the Standard Model and General Relativity, that passes all the particle physics and solar system tests.

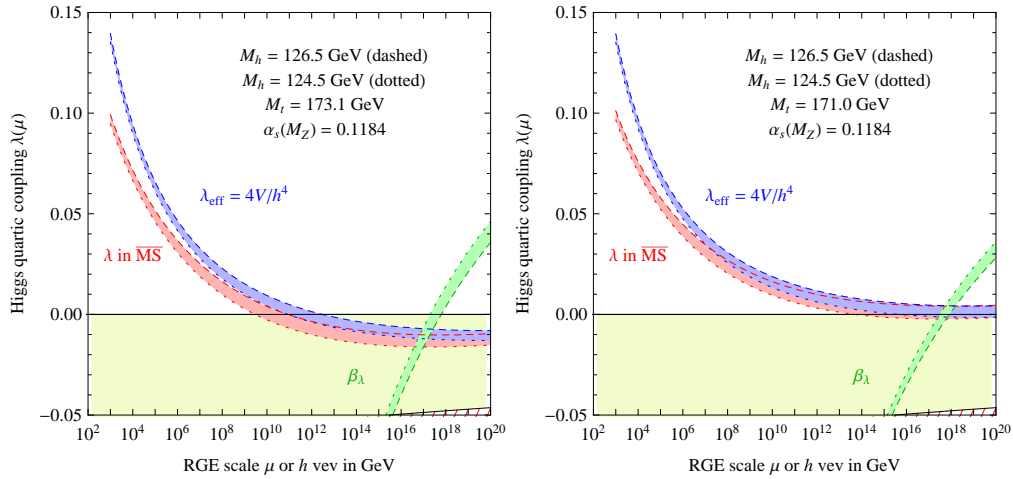


Figure 1. The RGE running of the Higgs quartic coupling $\lambda(\mu)$ for $M_h = 125.5 \pm 1$ GeV and different values of the top Yukawa coupling (left: $M_t = 173.1$ GeV; right: $M_t = 171.0$ GeV). Figures from Ref. [11].

(b) From the Jordan to the Einstein frame¹

Making a conformal metric transformation from the Jordan to the Einstein frame¹,

$$\tilde{g}_{\mu\nu} = \Omega^2 g_{\mu\nu} \equiv \frac{1}{M_P^2} (\xi_\chi \chi^2 + \xi_h h^2) g_{\mu\nu}, \quad (1.7)$$

¹ A tilde on a quantity indicates that it is expressed on the Einstein frame, where $\tilde{g}_{\mu\nu} = \Omega^2 g_{\mu\nu}$ and $\Omega^2 = M_P^{-2} f(h, \chi)$.

then the Lagrangian of Eq. (1.1), transforms into

$$\frac{\mathcal{L}}{\sqrt{-\tilde{g}}} = \frac{1}{2} M_P^2 \tilde{R} + \tilde{\mathcal{L}}_{\text{SM}[\lambda \rightarrow 0]} - \frac{1}{2} \tilde{K} - \tilde{U}(h, \chi), \quad (1.8)$$

where \tilde{K} is a non-canonical kinetic term, $\tilde{K} = \gamma_{ab} \tilde{g}^{\mu\nu} \partial_\mu \phi^a \partial_\nu \phi^b$, where γ_{ab} is in general non-diagonal, and non-canonical metric in the space of fields,

$$\gamma_{ab} = \frac{1}{\Omega^2} \left(\frac{3}{2} M_P^2 \frac{\partial_a \Omega^2 \partial_b \Omega^2}{\Omega^2} \right), \quad (1.9)$$

and $\tilde{U}(h, \chi)$ is the scalar potential,

$$\tilde{U}(h, \chi) = \frac{M_P^4}{(\xi_\chi \chi^2 + \xi_h h^2)^2} \left(\frac{\lambda}{4} \left(h^2 - \frac{\alpha}{\lambda} \chi^2 \right)^2 + \beta \chi^4 + \Lambda_0 \right). \quad (1.10)$$

It is then straightforward to find the classical ground states for $\alpha, \lambda, \xi_\chi, \xi_h > 0$. We do so first by finding them for the case where there is no cosmological constant Λ_0 , which in any case is very small, and second by observing in them the effect of a non-zero cosmological constant.

For $\Lambda_0 = 0$, then the theory reduces to Eq. (1.1), and the potential is minimal along the two valleys

$$h_0^2 = \left(\frac{\alpha}{\lambda} + \frac{4\beta\xi_h}{\lambda\xi_\chi + \alpha\xi_h} \right) \chi_0^2. \quad (1.11)$$

The effect of a non-zero Λ_0 is to give the valleys a tilt, which breaks the degeneracy of the classical ground states, no longer flat. Therefore, $\Lambda_0 > 0$ does not play the role of a cosmological constant but rather gives rise to a run-away potential for the scalar fields. Moreover, if $\beta = 0$, dark-energy does not contain a pure-constant contribution and is entirely generated by the term proportional to Λ_0 . This latter condition on β is assumed for the rest of the paper.

(c) Overview on Higgs-Dilaton cosmology

We will now proceed to describe the main features of the Higgs-Dilaton model.

- *Inflationary Era:* If the initial conditions of the scalar fields are far away from the potential valleys, they will roll slowly towards one of them. Λ_0 can be safely neglected as it is yet very small. This slow-roll of the fields is responsible for inflation, which, being driven by the Higgs field, is much like in the case of the Higgs-Inflation model of Ref. [4]. The era of inflation is eventually terminated by the reheating phase described in Ref. [5].
- *Preheating Phase:* After inflation, the scalar field dynamics is dominated by the field h . The gauge bosons created at the minimum of the potential acquire a large mass and starts to decay into all of the SM particles. The fraction of energy going into Standard Model particles is yet small, so non-perturbative decay is slow (see in Ref. [5]).
- *Reheating phase:* After some time, the amplitude of the oscillations becomes small enough that the gauge boson masses become too small to induce a quick decay, and their occupation numbers start to grow rapidly via parametric resonance. Then the gauge bosons back-react on the Higgs field and preheating ends. From there on, the Higgs field as well as the gauge fields decay perturbatively until their energy is transferred to SM leptons and quarks.
- *Dark-Energy Era:* After preheating and reheating the scalar fields satisfy Eq. (1.11) with $\beta = 0$, and remain virtually static for most of the present Universe history. The energy contained in the $h(t)$ and $\chi(t)$ fields stays almost unchanged, fixed at a given value by Λ_0 . Eventually it dominates the energy budget of the Universe as it scales with $\Omega_\Lambda \propto a^0$ while radiation and matter energy densities scale with $\Omega_r \propto a^{-4}$ and $\Omega_m \propto a^{-3}$, respectively.

The next two sections will now describe the HDM phenomenology of the Inflation and Dark-Energy Era in detail.

2. HDM Implications for the early Universe

Here we discuss the HDM predictions for the Inflationary Era. During inflation, all the energy of the Universe was contained in the inflaton and the gravitational fields, so one can readily neglect the Standard Model fields in the Lagrangian, $\tilde{\mathcal{L}}_{\text{SM}[\lambda \rightarrow 0]} \rightarrow 0$. In the Einstein-Frame, see Eq. (1.8), one is left with the scalar-tensor part, with $\tilde{U}(\phi) = \tilde{V}(\phi) + \tilde{V}_{\Lambda_0}(\phi)$, where we have expressed the Higgs and dilaton fields in a vector manner, for brevity, $\phi = (h, \chi)$.

Since inflation only takes place in the scale invariant region of the potential, one can neglect the scale-invariance breaking term Λ_0 . In the Einstein-Frame, as the metric $\tilde{g}_{\mu\nu}$ is scale-invariant by definition, scale transformations do not act on it and thus $\delta\tilde{g}_{\mu\nu} = 0$. This allows to redefine the fields as $\phi' = (\rho, \theta)$, which in terms of the original fields $\phi = (h, \chi)$ (see Ref. [2]), are

$$\rho = \frac{M_P}{2} \ln \left(\frac{(1 + 6\xi_\chi)\chi^2 + (1 + 6\xi_h)h^2}{M_P^2} \right) \quad (2.1)$$

$$\theta = \arctan \left(\sqrt{\frac{1 + 6\xi_h}{1 + 6\xi_\chi}} \frac{h}{\chi} \right), \quad (2.2)$$

so that the scale transformation only acts on a single field, ρ . Note that the argument of the logarithm in Eq. (2.1) is reminiscent of the 2D ellipse equation in the (h, χ) plane and can be interpreted as the radius ρ of the field vector ϕ , while from the argument of the arctangent in Eq. (2.2) is clear that θ can be interpreted as the the argument of the field vector ϕ . One may tentatively refer to this new variables as “polar fields” and we will do so throughout the rest of the paper.

(a) Evolution equations for the background

We now proceed to study the field trajectories during inflation in order to link the couplings of the theory with inflationary quantities. In a Friedmann-Lemaître-Robertson-Walker (FLRW) background,

$$ds^2 = \tilde{g}_{\mu\nu} dx^\mu dx^\nu = -dt^2 + a^2(t) d\mathbf{x}^2, \quad (2.3)$$

and following Ref. [2], the Friedmann and Klein-Gordon equations can be written, with comoving time expressed in terms of the e-fold parameter $N = \ln a(t)$, as²

$$H^2 = \frac{\tilde{U}}{3M_P^2 - |\phi'|^2/2}, \quad \frac{H'}{H} = -\frac{1}{2} \frac{|\phi'|^2}{M_P^2}, \quad (2.4)$$

$$-M_P^2 \nabla^\dagger \ln \tilde{U} = \phi' + \frac{D\phi'/dN}{3 - |\phi'|^2/2M_P^2}. \quad (2.5)$$

We will solve this equation in the slow-roll (SR) formalism.

(i) Slow-roll parameters

In the HDM, inflation occurs due to a phase of slow-roll of the scalar fields over an almost-flat potential long before the fields reach one of the potential valleys. It is then convenient (see

²A prime ' denotes a derivative w.r.t the number of e-folds.

Ref. [14]) to define the slow-roll parameter ϵ and the slow-roll vector η as

$$\epsilon \equiv -\frac{H'}{H} = \frac{1}{2} \frac{|\phi'|^2}{M_P^2}, \quad \eta \equiv \frac{1}{|\phi'|} \frac{D\phi'}{dN}, \quad (2.6)$$

where the vector notation is introduced due to the presence of more than one field in the model. Inflation ends when the slow-roll parameters cease to be smaller than unity or a phase transition occurs. Imposing the slow-roll conditions, in terms of the number of e-folds, the Friedmann Equations (2.4), and Klein-Gordon Equation (2.5) can now be rewritten as:

$$H^2 = \frac{\tilde{U}}{3M_P^2}, \quad \phi' = -M_P^2 \nabla^\dagger \ln \tilde{U}, \quad (2.7)$$

giving the evolution of the field vector ϕ .

(ii) Background trajectories

Lets discuss the regions in the (h, χ) -plane for which the approximate slow-roll conditions hold. The initial conditions for the trajectories must be chosen in the slow-roll region; the shape of the potential Eq. (1.10) attracts all trajectories to one of the potential valleys, and the roll starts. Some trajectories will leave the slow-roll region by reaching a steeper part of the potential valley and oscillate strongly around its minimum, allowing for a reheating phase to take place before settling in the potential valley.

As reheating is a necessary component of any viable theory of inflation, it is this class of trajectories to which we adhere for the rest of the analysis, constraining the initial conditions of the fields. For these trajectories, and in terms of the polar redefinition of the fields (ρ, θ) of Eqs. (2.1) and (2.2), the slow-roll equations for the scalar fields Eq. (2.7) become

$$\rho' = 0, \quad \theta' = -\frac{4\xi_\chi}{1 + 6\xi_\chi} \cot \theta \left(1 + \frac{6\xi_\chi \xi_h}{\kappa(\theta)} \right). \quad (2.8)$$

where $\kappa(\theta) = \xi_\chi \cos^2 \theta + \xi_h \sin^2 \theta$.

As a consequence of scale-invariance, the second scalar field equation in Eq. (2.8) does not depend on ρ_0 but only on θ . This ensures that there are no entropy perturbations in this model that may produce isocurvature fluctuations at reentry [13], which is quite positive for the HDM model since they are strongly constrained by *Planck* satellite (2015 data release) [15].

Integrating Eq. (2.8) up to the end of inflation, that is, from θ to θ_{end} , the number of e-folds is

$$N(\theta, \theta_{\text{end}}) = \frac{1}{4\xi_\chi} \ln \left(\frac{\cos \theta_{\text{end}}}{\cos \theta} \right) + \frac{3}{4} \ln \left(\frac{\kappa(\theta_{\text{end}}) + 6\xi_\chi \xi_h}{\kappa(\theta) + 6\xi_\chi \xi_h} \right), \quad (2.9)$$

where θ_{end} can be determined by finding its value when

$$\epsilon(\theta_{\text{end}}) = \frac{8\xi_\chi^2(1 + 6\xi_h)}{1 + 6\xi_\chi} \frac{\cot^2 \theta_{\text{end}}}{\kappa(\theta_{\text{end}})} = 1. \quad (2.10)$$

(b) Linear perturbations on the background

We will now calculate the scalar $\mathcal{P}_s(k)$ and tensor $\mathcal{P}_t(k)$ power spectra of perturbations from the evolution of the Higgs and dilaton fields, h and χ . This evolution is encoded in the slow-roll parameters ϵ and η , which ultimately depend on the theory couplings $\xi_h/\sqrt{\lambda}$ and ξ_χ .

We make use of the theory of cosmological perturbations emerging from quantum fluctuations during inflation, developed, among others, by Ref. [16]. Including scalar and tensor perturbations, and choosing the Newtonian transverse traceless gauge, the metric can be expanded in scalar (curvature) and tensor (gravitational waves) perturbations,

$$ds^2 = -(1 + 2\Phi) dt^2 + a(t)^2 [(1 - 2\Psi) \delta_{ij} + h_{ij}] dx^i dx^j, \quad (2.11)$$

where Φ and Ψ are the Bardeen potentials of Ref. [17]. Vector perturbations (vorticity) are not considered since they decay rapidly during inflation.

To compare the HDM with CMB observations, let us start with the power spectrum of the primordial scalar perturbations, (see Refs. [17] and [18]). The comoving curvature perturbation is $\zeta \equiv \Psi - \frac{H}{\dot{H}} (\dot{\Psi} + H\Phi)$. It can be shown [13,19] that ζ is conserved outside the horizon if inflation takes place in the scale-invariant region, just like in the single-field inflation scenario.

By making use of the slow-roll formalism, the amplitude $A_s(k)$ of the scalar power spectrum, $\mathcal{P}_s(k) = A_s(k/k_0)^{n_s-1}$, can be expressed as (see Ref. [16])

$$A_s(k) \simeq \frac{1}{2M_P^2 \epsilon} \left(\frac{H^*}{2\pi} \right)^2 \simeq \frac{\tilde{V}^*}{24\pi^2 \epsilon M_P^4}, \quad (2.12)$$

where quantities with an asterisk are evaluated at the moment of horizon crossing, that is, when $aH = k_0$. The scalar spectral index $n_s(k)$ is given by³

$$n_s(k) \equiv 1 + \frac{d \ln \mathcal{P}_s}{d \ln k} \simeq 1 - 2(\epsilon + \eta_{\parallel}), \quad (2.13)$$

and the running of the spectral index $\alpha_s(k)$ can be expressed as

$$\alpha_s \equiv \frac{dn_s}{d \ln k} \simeq -4\epsilon \eta_{\parallel} - 2\eta_{\parallel} \frac{d^2 \ln \epsilon}{dN^2}, \quad (2.14)$$

thus giving a non zero running.

The amplitude $A_t(k)$ of the power spectrum of the primordial tensor perturbations $\mathcal{P}_t(k) = A_t(k/k_0)^{n_t}$ can be written as

$$A_t(k) \simeq \frac{8}{M_P^2} \left(\frac{H^*}{2\pi} \right)^2 \simeq \frac{2\tilde{V}^*}{3\pi^2 M_P^4}, \quad (2.15)$$

which gives a tensor spectral index $n_t(k)$

$$n_t(k) \equiv \frac{d \ln \mathcal{P}_t}{d \ln k} \simeq -2\epsilon, \quad (2.16)$$

while we neglect the running of the tensor spectral index $\alpha_t = dn_t/d \ln k$.

Finally, it can be easily seen that the ratio of the tensor and the scalar spectra to first order in slow-roll is given by

$$r \equiv \frac{A_t}{A_s} \simeq 16 \epsilon = -8 n_t, \quad (2.17)$$

which gives a consistency condition, a relation that holds for the vast majority of single-field inflationary models in the slow-roll approximation, at least to the first non-trivial order.

(c) CMB constraints on parameters and predictions

Here we relate the observables of the CMB with the model couplings, via the primordial spectra. Since the whole period of observable inflation takes place in the scale-invariant region of the potential, we can use the background trajectories Eqs. (2.9) and (2.10) and directly compare to the primordial spectra calculated in Eqs. (2.12) and (2.15), and measured in the CMB, while assuming that during inflation entropy (isocurvature) perturbations are not excited, thanks to scale invariance [2].

We start by computing the spectral quantities $\mathcal{P}_s(k_0)$, $n_s(k_0)$, $\alpha(k_0)$ and $r(k_0)$ evaluated at the pivot scale k_0 , in terms of the HDM couplings ξ_χ , ξ_h and λ . First, we start by parametrically solving Eq. (2.10), giving the final state of the field θ_{end} at the end of the inflationary period, as a function of the HDM couplings. Second, the field θ_{end} is inserted into Eq. (2.9), parametrically solving as a function of the HDM couplings and obtaining θ^* , the state of the field at the moment where the modes k_0 exits the horizon during inflation. Third, the spectral quantities in Eqs. (2.12), (2.13), (2.14) and (2.17) are evaluated at θ^* to find the spectral quantities $\mathcal{P}_s(k_0)$, $n_s(k_0)$,

³For a formal definition of the speed-up rate η_{\parallel} and the turn rate η_{\perp} , see Ref. [2]. They are the components of the slow-roll parameter η in the parallel and perpendicular directions of the field trajectory, which define an orthonormal coordinate system of basis elements e_{\parallel} and e_{\perp} .

$\alpha_s(k_0)$ and $r(k_0)$, as functions of the HDM couplings and N^* , the number of e-folds between the moment where the modes k_0 exits the horizon and the end of inflation. Finally, N^* is expressed as a function of the HDM couplings, in order to check whether the model is able to provide with a number of e-folds large enough that the Horizon, Homogeneity and Relic Problems of w_0w_a CDM are solved.

Before we start, however, it can be shown that the number of e-folds roughly corresponds to

$$N^* \simeq 60 - \ln \frac{k_0 \text{Mpc}}{0.002 a_0} - \ln \frac{10^{16} \text{ GeV}}{\tilde{V}(\theta^*)^{1/4}} + \ln \left(\frac{\tilde{V}(\theta^*)}{\tilde{V}(\theta_{\text{end}})} \right)^{1/4} - \frac{1}{3} \ln \left(\frac{\tilde{V}(\theta_{\text{end}})}{\varrho_{\text{rh}}} \right)^{1/4}, \quad (2.18)$$

where ϱ_{rh} is the energy density at reheating. It has been found in Ref. [5] that reheating in Higgs Inflation is very efficient, and henceforth we take the approximation that a negligible number of e-folds occur during the reheating phase – that is, we consider the case on instantaneous reheating of Ref. [2] –, at θ_{end} . Then, $\varrho_{\text{rh}} = \tilde{V}(\theta_{\text{end}})$, and one thus has $\xi_\chi \lesssim 10^{-3}$ and $\xi_h/\sqrt{\lambda} \sim \mathcal{O}(10^4)$. With these bounds in mind, one can safely neglect second-order terms in ξ_χ , $1/\xi_h$ and, as will latter be seen, also in $1/N^*$, see Eq. (2.22).

Moving on the explicit computation of the spectral parameters in terms of this couplings, lets follow the above four steps. Solving Eq. (2.10) up to first-order in ξ_χ and $1/\xi_h$, one obtains that the state of the field θ at the end of the inflationary period is $\theta_{\text{end}} = 2 \times 3^{\frac{1}{4}} \sqrt{\xi_\chi}$. Solving Eq. (2.9) up to first-order in ξ_χ and $1/\xi_h$, the state of the field θ , as a function of the number of e-folds at the moment of horizon crossing, is $\theta^* \simeq \arccos(\exp -4\xi_\chi N^*)$. To evaluate the spectral observables $A_s(k_0)$, $n_s(k_0)$ and $\alpha_s(k_0)$, we insert θ^* into the definitions of the spectral quantities given in Eqs. (2.12), (2.13) and (2.14), and the consistency condition (2.17), to obtain

$$A_s(k_0) \simeq \frac{\lambda \sinh^2(4\xi_\chi N^*)}{1152\pi^2 \xi_\chi^2 \xi_h^2}, \quad n_s(k_0) \simeq 1 - 8\xi_\chi \coth(4\xi_\chi N^*), \quad (2.19)$$

$$\alpha_s(k_0) \simeq -32\xi_\chi^2 \text{csch}^2(4\xi_\chi N^*), \quad r(k_0) \simeq 192\xi_\chi^2 \text{csch}^2(4\xi_\chi N^*). \quad (2.20)$$

One can see that, in this approximation, $\alpha_s(k_0)$, $r(k_0)$ and $n_t(k_0)$ are related by

$$\alpha_s(k_0) \simeq -\frac{1}{6} r(k_0) = \frac{4}{3} n_t(k_0), \quad (2.21)$$

which can be interpreted as an new consistency condition for the HDM that is specific to this inflationary theory.

In order to find N^* in terms of the parameters of the theory, we insert θ^* into Eq. (2.18), giving the approximate result

$$N^* \simeq 65 - \frac{1}{2} \ln \frac{\xi_h}{\sqrt{\lambda}} \approx 60, \quad (2.22)$$

which is compatible with solving the Homogeneity, Horizon and Relic Problems of w_0w_a CDM and allows to neglect second order terms in $1/N^*$ in Eqs. (2.19) and (2.20).

This result also provides a limit on the reheating temperature T_{rh} , defined as the initial temperature of the homogeneous radiation dominated universe. T_{rh} is related to ϱ_{rh} through

$$\varrho_{\text{rh}} = \frac{\pi^2}{30} g_{\text{eff}}(T_{\text{rh}}) T_{\text{rh}}^4, \quad (2.23)$$

where $g_{\text{eff}}(T_{\text{rh}}) = 107.75$ is the effective number of relativistic degrees of freedom of the Standard Model ($427/4 = 106.75$, plus 1 for the dilaton). This translates into the following upper and lower bounds on the reheating temperature of (see Ref. [2])

$$10^{12} \text{ GeV} \lesssim T_{\text{rh}} \lesssim 10^{15} \text{ GeV}. \quad (2.24)$$

Note that this extra relativistic degree of freedom could in principle add to the effective number of light degrees of freedom in the Universe. This would affect the Big Bang Nucleosynthesis (BBN) ratios for the observed element frequencies, and lay waste to one of the more accurate predictions of w_0w_a CDM. However, it can be shown that this is not the case since just after

reheating ends the dilaton energy density is of order $\mathcal{O}(10^{-7})$, i.e. virtually negligible, so it no longer contributes to the effective number of light degrees of freedom, as shown in Ref. [3].

3. HDM Implications for the late Universe

In this section we show that the dilaton is a good candidate for quintessence (QE), that is, a dynamical dark energy (DE) candidate, and provide with testable relations between CMB observables and the dark-energy equation of state parameter.

After the phase of reheating, the system enters the radiation dominated stage, at the beginning of which the total energy density is given by ϱ_{rh} , see Eq. (2.23). At this moment the scalar fields have nearly settled down in one of two potential valleys, $h(t)^2 \simeq (\alpha/\lambda)\chi(t)^2$. One could further redefine the polar variables introduced in Eqs. (2.1) and (2.2) by

$$\tilde{\rho} = \rho/\gamma, \quad |\tilde{\phi}| = |\phi_0| - \frac{M_P}{a} \operatorname{arctanh}(\sqrt{1-\zeta} \cos \theta), \quad (3.1)$$

where we have defined $a = \sqrt{\frac{\xi_x(1-\zeta)}{\zeta}}$ and $\gamma = \sqrt{\frac{\xi_x}{1+6\xi_x}}$. This new redefinition allows one to express the symmetry-breaking approximate ground states, that is, the two potential valleys, as a simple function of $\tilde{\theta}$ and the scalar curvature perturbation ζ

$$\tanh^2\left(\frac{a\tilde{\theta}(t)}{M_P}\right) \simeq 1 - \zeta. \quad (3.2)$$

We assume that the fields roll exactly at the bottom of the valley. In this case, $\tilde{\theta}$ is time-independent, and inserting the constraint (3.2) in the Einstein-Frame Lagrangian (1.8),

$$\frac{\mathcal{L}}{\sqrt{-g}} \simeq \frac{1}{2} M_P^2 \tilde{R} - \frac{1}{2} (\partial \tilde{\rho})^2 - \tilde{V}_{\text{QE}}(\tilde{\rho}), \quad (3.3)$$

where $V_{\text{QE}}(\tilde{\rho})$ is thawing quintessence-like potential, see Ref. [1]

$$\tilde{V}_{\text{QE}}(\tilde{\rho}) = \frac{A_0}{\gamma^4} e^{-4\gamma\tilde{\rho}/M_P}, \quad (3.4)$$

of the run-away kind that allows the dilaton field to play the role of a dynamic dark energy. For an interesting discussion of thawing and freezing Dark Energy models and a comparison between various parametrizations see Ref. [20].

Lets now discuss in more detail the influence of the field $\tilde{\rho}$ on standard homogeneous cosmology. In the FLRW metric, the equation of motion for the homogeneous dynamic field $\tilde{\rho}(t)$ is given by $\ddot{\tilde{\rho}} + 3H\dot{\tilde{\rho}} + \frac{dV_{\text{QE}}}{d\tilde{\rho}} = 0$. The equation of state parameter w_i of any perfect fluid “ i ” is $w_i \equiv p_i/\varrho_i$, and so for the scalar field $\tilde{\rho}$ it is

$$w_{\text{QE}} \equiv \frac{p_{\text{QE}}}{\varrho_{\text{QE}}} \equiv \frac{\dot{\tilde{\rho}}^2/2 - V_{\text{QE}}}{\dot{\tilde{\rho}}^2/2 + V_{\text{QE}}}, \quad (3.5)$$

and thus the equation of motion of dark energy can be more compactly written as $\dot{\varrho}_{\text{QE}} = -3H\varrho_{\text{QE}}(1 + w_{\text{QE}})$. Also, for a barotropic fluid of energy density ϱ_b , the Hubble parameter is given by the first Friedmann Equation as $H^2 = (\varrho_b + \varrho_{\text{QE}})/(3M_P^2)$, which in terms of the relative abundances $\Omega_i = \varrho_i/(3M_P^2 H^2)$ for a perfect fluid “ i ” can be written as the cosmic sum rule $\Omega_{\text{m}} + \Omega_{\text{QE}} = 1$, for flat space, neglecting the radiation and neutrino contributions.

It is useful to rewrite these equations in terms of the dark-energy energy density, Ω_{QE} , and deviation from pure cosmological constant parameter, $\delta_{\text{QE}} \equiv 1 + w_{\text{QE}}$. The scalar field evolution equation and the Friedmann Equation can then be written as

$$\delta'_{\text{QE}} = (2 - \delta_{\text{QE}}) \left(-3\delta_{\text{QE}} + 4\gamma\sqrt{3\delta_{\text{QE}}\Omega_{\text{QE}}} \right), \quad (3.6)$$

$$\Omega'_{\text{QE}} = 3(\delta_i - \delta_{\text{QE}})(1 - \Omega_{\text{QE}})\Omega_{\text{QE}}. \quad (3.7)$$

Defining $\delta_i \equiv 1 + w_i$, where the sub-index “ i ” stands for any barotropic fluid, be it radiation “ r ” or matter “ m ”, it follows immediately that radiation has $p_r = \rho_r/3 \Rightarrow w_r = 1/3$, so $\delta_r = 4/3$; dust has $p_m = 0 \Rightarrow w_m = 0$, so $\delta_m = 1$. A pure cosmological constant holds exactly that $p_\Lambda = -\rho_\Lambda \Rightarrow w_\Lambda = -1$, so $\delta_\Lambda = 0$. A more general dark energy component only needs $p_{\text{DE}} < -\rho_{\text{DE}}/3 \Rightarrow w_{\text{DE}} < -1/3$, so $\delta_{\text{DE}} < 2/3$. In Refs. [21] and [22] it is shown that, for $0 \leq \delta_b \leq 2$, the field trajectories approach one of two different attractor solutions. Which of these two depends on the value of γ : If $4\gamma > \sqrt{3\delta_i}$, the field evolution is driven towards a stable fixed point $\Omega_{\text{QE}} = 3\delta_i/16\gamma^2$ with $\delta_{\text{QE}} = \delta_i$. In this case, the scalar field can only account at best for a small contribution to dark-energy as it gives rise to a baryon-like equation of state parameter, $w_{\text{QE}}(\gamma > \sqrt{3\delta_i}/4) = 1$. If $4\gamma < \sqrt{3\delta_i}$, the field evolution is driven towards a different stable fixed point $\Omega_{\text{QE}} = 1$ with $\delta_{\text{QE}} = 16\gamma^2/3$. the scalar field can in this case describe the late-time acceleration of the Universe since it develops an equation of state parameter $w_{\text{QE}}(\gamma < \sqrt{3\delta_i}/4) = 16\gamma^2/3 - 1$, less than $-1/3$ if $\gamma < \sqrt{3\delta_i}/4$ or alternatively $\xi_\chi < 1/2$.

It was found in section 2 that the Higgs-Dilaton model is able to describe inflation as long as the coupling of the dilaton field to gravity is much smaller than unity, i.e. $\xi_\chi \lesssim 10^{-2}$, so that cosmological trajectories are ensured to approach the second attractor, and accelerated expansion of the Universe is bound to occur.

(a) Dark-energy constraints on parameters and predictions

We now proceed to give the explicit dependence of the equation of state parameters and the couplings of the theory, just as in the previous section the same was done for the scalar and tensor power spectra. It was shown in subsection 1(a) that for the case where the potential in Eq. (1.10) had $\beta = 0$, all of the dark-energy would consist of the $\tilde{\rho}$ scalar field energy density and be analogous to quintessence, while for the case with $\beta \neq 0$, dark energy would have an additional contribution from the cosmological constant term, Λ_0 . In this paper no distinction is being made, however, between quintessence and dark energy, as we are operating under the first assumption, and for the rest of the analysis we switch from “QE” to “DE” as the corresponding label for quintessence/dark energy observables.

The Inflationary era is followed by the Radiation and Matter dominated eras. During this epoch, the second term on the right-hand side of Eq. (3.6) is small compared to the first one δ_{DE} is set at an equation of state parameter virtually indistinguishable from a pure cosmological constant, $w_{\text{DE}} \simeq -1$, yet of low energy density. However, since the energy density of quintessence barely decreases over time, Ω_{DE} eventually becoming relevant. It is then when the scalar fields $\tilde{\rho}$ starts rolling faster down the potential valleys and δ_{DE} starts growing towards its attractor value, driving the accelerated expansion of space.

Note that while the Universe is not yet purely quintessence-dominated, $\delta_{\text{DE}} \ll 1$, Eqs. (3.6) and (3.7) yield (for a detailed calculation, see Ref. [23]) $3\delta_{\text{DE}} \simeq 16\gamma^2 F^2(\Omega_{\text{DE}})$, where F is the function defined below,

$$F(\Omega_{\text{DE}}) \equiv \frac{\Omega_{\text{DE}} + 2\sqrt{\Omega_{\text{DE}}} - 1}{2\Omega_{\text{DE}}} \ln \frac{1 + \sqrt{\Omega_{\text{DE}}}}{1 - \sqrt{\Omega_{\text{DE}}}}, \quad (3.8)$$

increasing from $F(0) = 0$ in the Radiation and Matter eras to $F(1) = 1$ when quintessence becomes fully dominant. Note that we are finally able to link the inflationary quantities with dark energy observables, and it can be shown in particular that, for $\xi_\chi \lesssim 10^{-3}$, then $\delta_{\text{DE}} \lesssim 10^{-2}$ as well.

(b) Constrain relations between early and late Universe observables

We finally arrive to the point where three expressions, one linking first order parameters w_{DE}^0 and $n_s(k_0)$, another linking second order parameters w_{DE}^a and $\alpha_s(k_0)$, and one last on $r(k_0)$ and w_{DE}^0 are deduced. These can be understood as consistency checks on the model, since they put very stringent bounds on the predicted values of $r(k_0)$ and w_{DE}^0 respectively.

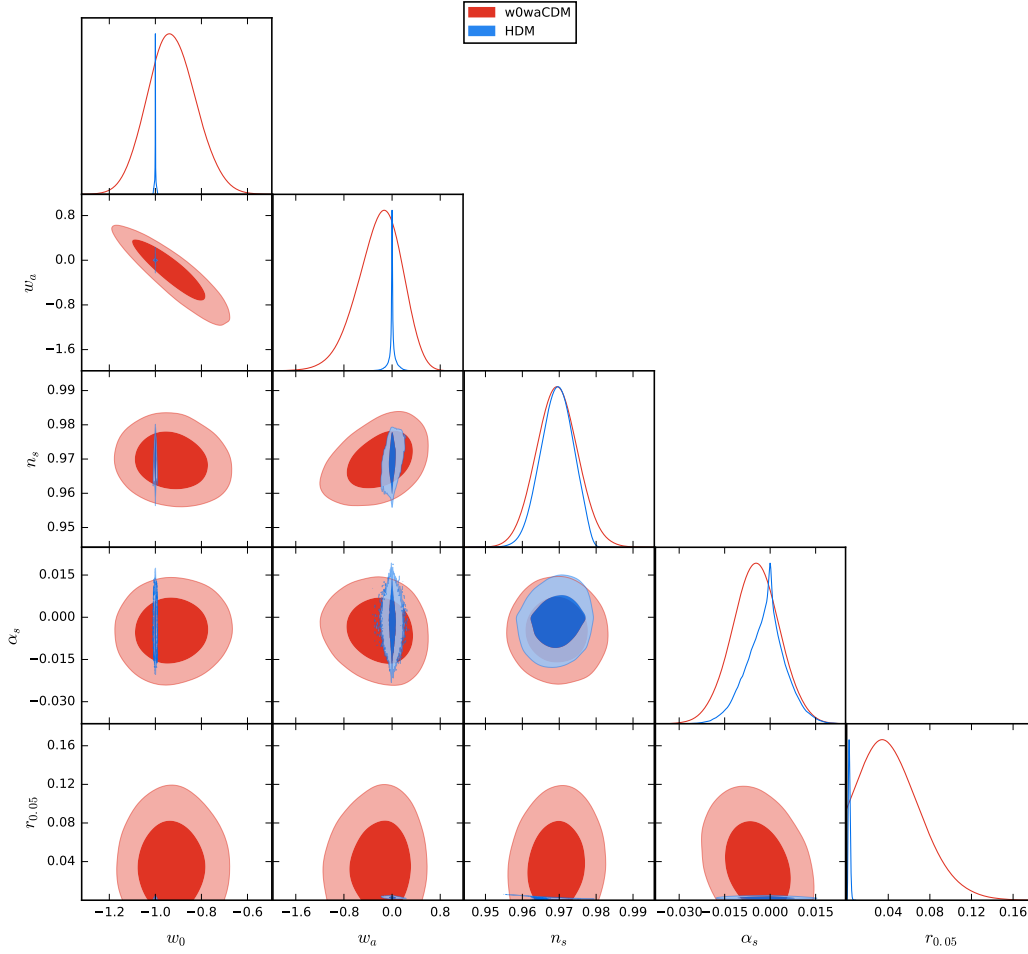


Figure 2. 1σ and 2σ contour plots for w_{DE}^0 , w_{DE}^a , n_s , α_s , and $r_{0.05}$ for the HDM (blue) and $w_0w_a\text{CDM}$ model (red), showing the great extent to which the HDM constrains the available cosmological parameter space for the tensor-to-scalar ratio $r_{0.05}$ as well as for the dark energy equation of state parameters w_{DE}^0 and w_{DE}^a .

(i) First-order consistency relations

We can test the constraint relation between the scalar spectral index n_s and the equation of state parameter w_{DE}^0 as they both depend on ξ_χ , for a given number of e-folds N_{inf} . Lets then find the explicit relation between these magnitudes. One can write the scalar tilt n_s as a function the quintessence equation of state parameter δ_{DE} and the number of e-folds N_{inf} ,

$$n_s = 1 - \frac{2}{N_{\text{inf}}} G \coth G, \quad (3.9)$$

where the function $G(\Omega_{\text{DE}}, \delta_{\text{DE}})$ is defined as

$$G(\Omega_{\text{QE}}, \delta_{\text{DE}}, N_{\text{inf}}) = \frac{6\delta_{\text{DE}}N_{\text{inf}}}{8F(\Omega_{\text{QE}}) - 9\delta_{\text{DE}}}, \quad (3.10)$$

so a relationship between n_s and w_{QE}^0 can be established, and it is enough to replace $\delta_{\text{DE}} = 1 + w_{\text{DE}}$ in Eq. (3.9), which for the case where $\delta_{\text{DE}} \rightarrow 0$ reduces to $n_s \rightarrow 1 - 2/N_{\text{inf}}$. This result

can be written as the differential expression

$$\left. \frac{d \ln \varrho_{\text{QE}}}{d \ln a} \right|_{a^*} \simeq \left. \frac{d \ln P_s(k)}{d \ln k} \right|_{k_0}, \quad (3.11)$$

at horizon reentry, that is, when $k_0 = a^* H$. Note that the last equation, being a relation between the very small and the very big scales, implies a linear relation between the deviations from scale invariance in n_s and the deviations from the pure cosmological constant dark energy equation of state parameter δ_{DE} , which can be understood as a consequence of scale invariance.

(ii) Second-order consistency relations

We can also test a constraint relation involving second order quantities: the running of the scalar spectral index α_s , the equation of state parameter w_{DE}^0 , and its running with the scale factor, w_{DE}^a , again as they both depend on ξ_X , for a given number of e-folds N_{inf} .⁴

$$\alpha_s = -\frac{8w_{\text{DE}}^a F}{3\delta_{\text{DE}} N_{\text{inf}}^2} G^2 \left(\text{csch}^2 G - G \coth G^2 \right), \quad (3.12)$$

which for the case where $\delta_{\text{DE}} \rightarrow 0$ reduces to $\alpha_s \rightarrow 0$, which can also be considered as a consistency check for the theory, albeit a second order one, whose testability however may still have to wait for a longer time than for the first-order case since they are as of yet very poorly constrained. Also, in a similar manner, we have the equivalent relation for the second order quantities

$$\left. \frac{d^2 \ln \varrho_{\text{DE}}}{(d \ln a)^2} \right|_{a^*} \simeq \left. \frac{d^2 \ln \mathcal{P}_s(k)}{(d \ln k)^2} \right|_{k_0}, \quad (3.13)$$

at horizon reentry, that is, when $k_0 = a^* H$. This is again a non trivial result that, just as in the case of the first-order relation, may be understood as a consequence of scale invariance.

Table 1. Constraints on cosmological parameters $\Omega_b h^2$, $\Omega_c h^2$, $100\theta_{\text{MC}}$, τ_{RE} , w_{DE}^0 , w_{DE}^a , $\ln(10^{10} A_s)$, n_s , α_s , $r_{0.05}$ and N_{inf} , using the data sets described in the text *BKP+len.+lowl+MPK+ext.*, for the $w_0 w_a$ CDM and HDM COSMOMC chains at the 68.3% and 95.5% confidence levels.

Parameter	$w_0 w_a$ CDM		HDM	$w_0 w_a$ CDM	
	68.3% c.l.			95.5% c.l.	
$\Omega_b h^2$	0.02237 ± 0.00025	0.02233 ± 0.00022		$0.02237^{+0.00051}_{-0.00049}$	$0.02233^{+0.00044}_{-0.00043}$
$\Omega_c h^2$	0.1177 ± 0.0018	0.1177 ± 0.0013		0.1177 ± 0.0035	$0.1177^{+0.0025}_{-0.0025}$
$100 \theta_{\text{mc}}$	1.04111 ± 0.00045	1.04106 ± 0.00040		1.04111 ± 0.00088	$1.04110^{+0.00083}_{-0.00082}$
τ_{re}	$0.069^{+0.017}_{-0.019}$	0.066 ± 0.013		$0.069^{+0.038}_{-0.035}$	$0.070^{+0.027}_{-0.027}$
$\ln(10^{10} A_s)$	$3.067^{+0.032}_{-0.036}$	3.068 ± 0.026		$3.067^{+0.069}_{-0.064}$	$3.068^{+0.050}_{-0.050}$
w_0	-0.93 ± 0.10	-1.0001 ± 0.0032		$-0.93^{+0.21}_{-0.20}$	$-1.0001^{+0.0072}_{-0.0074}$
w_a	$-0.21^{+0.41}_{-0.31}$	$0.001^{+0.039}_{-0.034}$		$-0.21^{+0.69}_{-0.74}$	$0.00^{+0.15}_{-0.16}$
n_s	0.9694 ± 0.0056	$0.9693^{+0.0046}_{-0.0042}$		0.969 ± 0.011	$0.9693^{+0.0083}_{-0.0082}$
α_s	-0.0047 ± 0.0078	-0.0014 ± 0.0066		-0.005 ± 0.015	$-0.001^{+0.013}_{-0.014}$
$r_{0.05}$	$0.045^{+0.017}_{-0.038}$	$0.00255^{+0.0007}_{-0.0010}$		< 0.0964	$0.0025^{+0.0017}_{-0.0016}$
N_{inf}	—	70^{+9}_{-10}		—	70^{+20}_{-20}

⁴We have chosen the following parametrization of the equation of state parameter for dark energy in terms of the scale factor: $w_{\text{DE}}(a) = w_{\text{DE}}^0 + w_{\text{DE}}^a \ln(a/a_0)$. Note the evolution is logarithmic, not linear, which is taken into account when implementing the two consistency relations in COSMOMC.

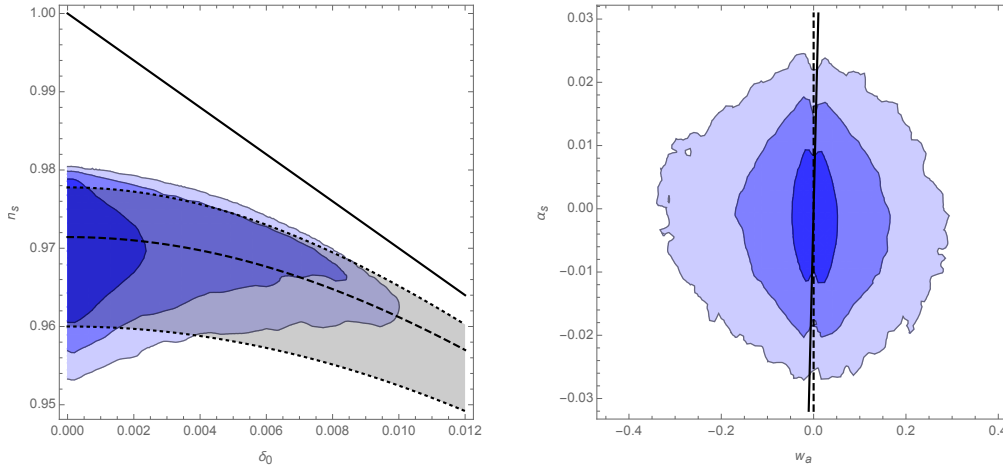


Figure 3. 1σ , 2σ and 3σ contours of $(1 + w_{\text{DE}}, n_s)$ (left) and $(w_{\text{DE}}^a, \alpha_s)$ (right) for the HDM. The solid line corresponds to the asymptotic solutions $n_s = 1 - 3(1 + w_{\text{DE}})$ (left) and $\alpha_s = 3w_{\text{DE}}^a$ (right). In both plots, the dashed line corresponds to the expressions of n_s and α_s in Eqs. (3.9) and (3.12) for the case of $N_{\text{inf}} = 70$ while the dotted lines corresponds to the expressions of n_s and α_s in Eqs. (3.9) and (3.12) for the 2σ bounds on the number of e-folds, that is $N_{\text{inf}} = 50$ (lower bound) and $N_{\text{inf}} = 90$ (upper bound) respectively.

(iii) Constraints on the tensor-to-scalar ratio

There is an additional constraint for the tensor-to-scalar ratio arising from Eq. (2.20), which, in terms of the energy density and equation of state parameters of dark energy reduces to:

$$r = \frac{12}{N_{\text{inf}}^2} G^2 \text{csch}^2 G, \quad (3.14)$$

which for the case where $\delta_{\text{DE}} \rightarrow 0$ reduces to $r \rightarrow 12/N_{\text{inf}}^2$. Note that the value of the tensor-to-scalar ratio r will very rapidly go to zero for a sufficiently large number of e-folds, and indeed, considering the previously found value of $N_{\text{inf}} \gtrsim 60$ and *Planck* satellite (2015 data release) best fit values for parameters Ω_{DE} and δ_{DE} , it can be easily checked that the HDM prediction for the tensor-to-scalar ratio is indeed extremely constraining, at $r \lesssim 10^{-2}$, a very interesting feature of the theory that may be tested in the not-so-far future.

(iv) Constraints on the HDM couplings

As a consequence, we find the constraints for the HDM couplings $\xi_h/\sqrt{\lambda}$ and ξ_χ by numerically inverting Eqs. (2.19) and (2.20),

$$\xi_\chi < 0.00109 \quad (0.00328) \quad \text{at } 68\% \text{ (95.5\%) c.l.} \quad (3.15)$$

$$\xi_h/\sqrt{\lambda} = 59200_{-14000}^{+6100} \quad ({}_{-20000}^{+30000}) \quad \text{at } 68\% \text{ (95.5\%) c.l.} \quad (3.16)$$

Finally, we present the 68.3% and 95.5% confidence contours for ξ_χ and $\xi_h/\sqrt{\lambda}$ on Figure 3. As it can be seen, there is significant improvement over the predictions of the confidence intervals with respect to Ref. [2].

To summarize this part of the work on HDI, we have found that the Higgs-Dilaton model is a viable extension of the Standard Model, based only on scale invariance and a non-minimal coupling to Unimodular Gravity, and is able to produce an early-Universe period of inflation, as well as explaining the present era of accelerated expansion. We have compared this model to the cosmological constant (Λ CDM) and evolving Dark Energy ($w_0 w_a$ CDM) models, by using the latest cosmological data that includes the Cosmic Microwave Background temperature,

polarization and lensing data from the *Planck* satellite, the BICEP and Keck Array experiments, the Type Ia supernovae from the JLA catalog, the Baryon Acoustic Oscillations and finally, the Weak Lensing data from the CFHTLenS survey, by implementing the model constraints in COSMOMC, a MCMC code.

Note that the relations between the observables from inflation, n_s and α_s , and from dark-energy era, w_{DE}^0 and w_{DE}^a , are very specific predictions of the model, that connect two seemingly independent epochs, and establish a measurable relation between observables from CMB anisotropies with the largely unknown dark-energy sector.

We found that the values of all cosmological parameters allowed by the Higgs-Dilaton model Inflation are well within the $w_0 w_a$ CDM constraints. In particular, we found that $w_{\text{DE}}^0 = -1.0001^{+0.0072}_{-0.0074}$, $w_{\text{DE}}^a = 0.00^{+0.15}_{-0.16}$, $n_s = 0.9693^{+0.0083}_{-0.0082}$, $\alpha_s = -0.001^{+0.013}_{-0.014}$ and $r_{0.05} = 0.0025^{+0.0017}_{-0.0016}$ (95.5% c.l.). We also placed new stringent constraints on the couplings of the Higgs-Dilaton model to gravity and found that $\xi_\chi < 0.00328$ and $\xi_h/\sqrt{\lambda} = 59200^{+30000}_{-20000}$ (95.5% c.l.). All of these are very relevant predictions of the model that may soon be confronted with observational data by *DES*, *PAU* and *Euclid*.

Furthermore, we found that the HDM is at a slightly better footing than the $w_0 w_a$ CDM model, as they both have practically the same *chi-square*, i.e. $\Delta\chi^2 = \chi_{w_0 w_a \text{CDM}}^2 - \chi_{\text{HDM}}^2 = 0.18$, but with the HDM model having two parameters less, and finally a Bayesian evidence favoring equally the two models.

4. Critical Higgs Inflation, CMB and Particle Physics

The first direct detection of gravitational waves (GWs) by LIGO has initiated a new era of astronomy [24] and opened the possibility to test the nature of dark matter, specially if its dominant component is primordial black holes (PBH) [25]. These massive black holes could arise in the early universe from the gravitational collapse of matter/radiation on large-amplitude curvature fluctuations generated during inflation [26,27]. All that is required is a super-slow-roll period (i.e. a plateau feature in the potential) during which the inflaton quantum fluctuations get amplified and produce a peak in the spatial curvature power spectrum [28,29]. The mass and spin distribution of the subsequently produced PBH then depends on the details of the inflationary dynamics. Its detection and characterization by LIGO, VIRGO and future GW detectors will allow us to open a new window into the physics of the early universe.

The nature of the inflaton field responsible for the initial acceleration of the universe is still unknown. Observations of the temperature and polarization anisotropies in the cosmic microwave background (CMB) suggests a special inflaton dynamics, dominated by a flat plateau on large scales [30]. Such type of potentials arise naturally in models of Higgs Inflation [31], where the scalar field responsible for inflation is the Higgs boson of the Standard Model (SM) of Particle Physics, with its usual couplings to ordinary matter (gauge fields, quarks and leptons), plus a new non-minimal coupling ξ to gravity. This economical scenario not only passes all solar system and CMB observational constraints, but also predicts a small tensor-to-scalar ratio and a large reheating temperature [32].

It has recently been realized [33] that the running of the Higgs self-coupling to large energy scales, via the renormalization group equations (RGE) within the 2σ SM values, could lead to a critical point $\phi_c = \mu$, with $\lambda(\mu) = \beta_\lambda(\mu) = 0$, where $\lambda(\phi)$ has a minimum, see Fig. 1. This induces an extra feature in the inflationary potential that could lead to a brief plateau of super-slow-roll conditions at scales much smaller than those of the CMB, giving rise to a large peak in the matter power spectrum, and thus to copious production of PBH.

We explore here the critical Higgs scenario, taking into account both the RGE running of the Higgs self-coupling and its non-minimal coupling to gravity [34]. The action of the Higgs-inflaton model is given by, where we have defined $\kappa^2 \equiv 8\pi G$,

$$S = \int d^4x \sqrt{g} \left[\left(\frac{1}{2\kappa^2} + \frac{\xi(\phi)}{2} \phi^2 \right) R - \frac{1}{2} (\partial\phi)^2 - \frac{1}{4} \lambda(\phi) \phi^4 \right], \quad (4.1)$$

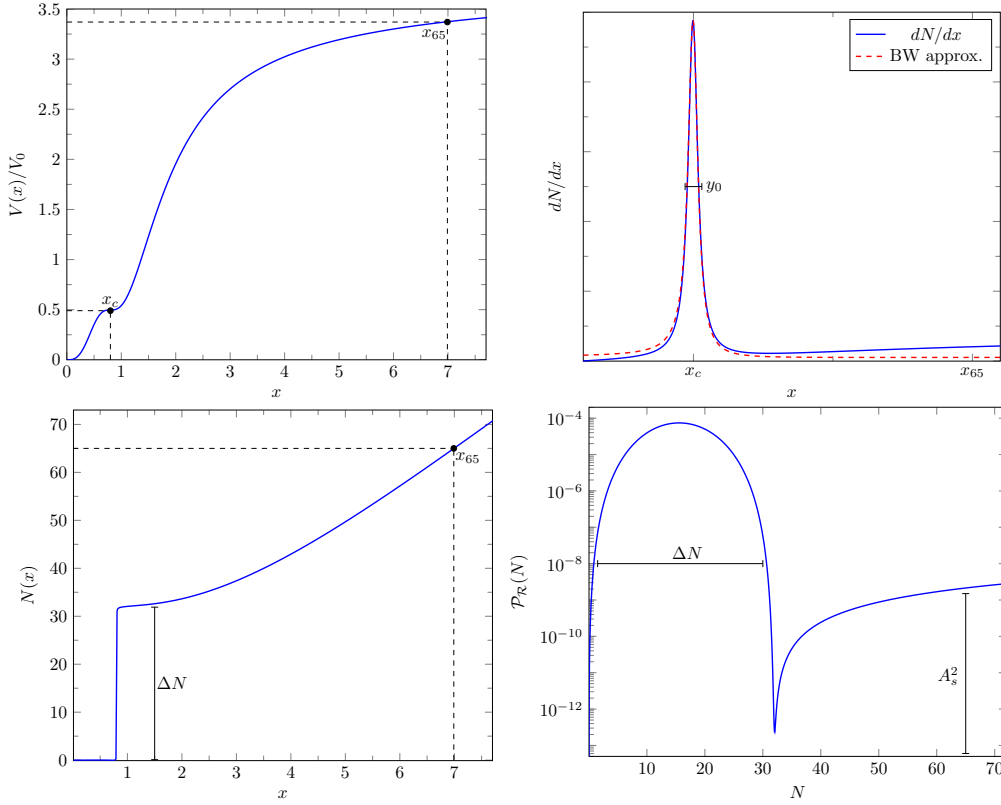


Figure 4. Top left panel: The CHI model potential with the quasi-inflection point at $x_c = \phi_c/\mu$. Top right panel: The spike in dN/dx with the Breit-Wigner approximation. Bottom left panel: The integrated number of e -folds, with the jump ΔN at the critical point. Bottom right panel: The curvature power spectrum $\mathcal{P}_{\mathcal{R}}(N)$. The large and broad peak at small scales ($N < \Delta N$) is responsible for PBH production over a wide range of masses.

with the running of the couplings parametrized by

$$\lambda(\phi) = \lambda_0 + b_\lambda \ln^2(\phi/\mu), \quad \xi(\phi) = \xi_0 + b_\xi \ln(\phi/\mu), \quad (4.2)$$

around the critical point $\phi = \mu$. After a standard metric and scalar field redefinitions ($\kappa^2 \equiv 1$),

$$\tilde{g}_{\mu\nu} = (1 + \xi(\phi)\phi^2) g_{\mu\nu}, \quad \varphi = \int \frac{d\phi}{1 + \xi(\phi)\phi^2} \left[1 + \xi(\phi)\phi^2 \left(1 + 6\xi(\phi) \left(1 + \frac{\xi_{,\phi}\phi}{2\xi} \right) \right) \right]^{1/2},$$

the effective inflationary potential becomes

$$V(x) = \frac{V_0 (1 + a \ln^2 x) x^4}{(1 + c(1 + b \ln x) x^2)^2}, \quad (4.3)$$

with $V_0 = \lambda_0 \mu^4/4$, $a = b_\lambda/\lambda_0$, $b = b_\xi/\xi_0$ and $c = \xi_0 \kappa^2 \mu^2$. The potential has a flat plateau at large values of the field $x = \phi/\mu$, see Fig. 4, where $V(x \gg x_c) \simeq V_0 a/(bc)^2 = 1/(4\kappa^4) (b_\lambda/b_\xi^2) \ll M_{\text{P}}^4$. Thus the small value of H_{inf} w.r.t. M_{P} is *only* determined by the RGE running of the SM Higgs couplings λ and ξ . The potential also has a short secondary plateau around the critical point, $\phi \simeq \mu$, where the inflaton-Higgs suffers super-slow-roll and induces a large peak in the curvature power spectrum. This second plateau is induced by a near-inflection point at $x = x_c$, where $V'(x_c) \simeq 0$, $V''(x_c) \simeq 0$. As a consequence, the number of e -folds has a sharp jump at that point, ΔN , plus a slow rise towards larger field values, corresponding to CMB scales. This potential and power spectrum is very similar to the one discussed in Ref. [28]. Following this reference, we have computed the tensor-to-scalar ratio, the scalar spectral index and its running at those scales, as well as the height of the peak at the critical point as a function of the model parameters.

We chose to parametrize the model in terms of the height and width of the peak in the power spectrum, see Fig. 4. The height of the peak relative to the amplitude at CMB scales (A_s^2) is controlled by the closeness of x_c to a true inflection point, $V'(x_c) = V''(x_c) = 0$. The width is determined by the jump in the number of e -folds, ΔN . There will be an inflection point at x_c if

$$a(x_c, c) = \frac{4}{1 + cx_c^2 + 2 \ln x_c - 4 \ln^2 x_c} \quad b(x_c, c) = \frac{2(1 + cx_c^2 + 4 \ln x_c - 4 \ln^2 x_c)}{cx_c^2(1 + cx_c^2 + 2 \ln x_c - 4 \ln^2 x_c)}. \quad (4.4)$$

Thus, a near-inflection can be characterized by $a \rightarrow a(x_c, c)$ and $b \rightarrow (1 - \beta)b(x_c, c)$. Then, the relative height of the peak will be proportional to β^{-1} and $\Delta N \propto \beta^{-1/2}$. Fixing β and ΔN , we compute the rest of parameters as a function of just two (x_c, c) , which we vary satisfying the 2σ CMB constraints.

We have studied the main CMB observables (the scalar spectral index n_s , its running, $\alpha_s = dn_s/d \ln k$, and the tensor-to-scalar ratio r), as a function of (x_c, c) , for different heights and widths. We find that, for each β and ΔN , there are many choices of (x_c, c) that give rise to valid cosmologies. In order to study the PBH production, we have chosen a reference one, $\beta = 7 \times 10^{-5}$, $\Delta N = 32$ and $(x_c, c) = (0.78, 0.48)$, for which the CMB parameters are $n_s = 0.9566$, $r = 0.028$ and $\alpha_s = -0.00144$, perfectly within the 2σ limits of Planck 2015 [30].

We present in Fig. 5 the results in the (n_s, r) -plane. The parameter space is consistent with CMB anisotropies, and at the same time induces a large peak in the power spectrum at small scales, that will later give rise to PBH through gravitational collapse upon reentry [26]. The peak can be parametrized by the ratio $\mathcal{P}_{\mathcal{R}}(x_c)/\mathcal{P}_{\mathcal{R}}(x_{65})$ of the amplitude of the fluctuations around the near-inflection point x_c over the one at the inflationary plateau x_{65} , which we find to be greater than 10^4 in the whole range of Fig. 5.

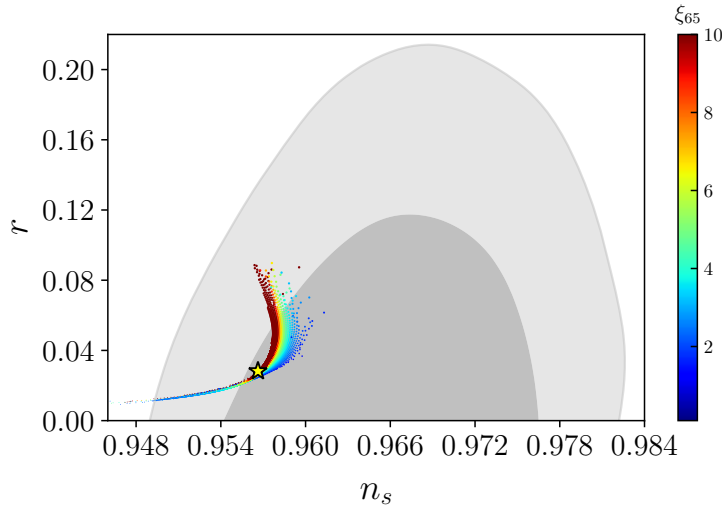


Figure 5. Predictions in the plane (n_s, r) of CHI with a large peak in the spectrum ($\beta = 7 \times 10^{-5}$ and $\Delta N = 32$). The color bar codes the value of the non-minimal coupling $\xi_{65} = \xi(\phi_{65})$ at CMB scales. The contours represent the 1 and 2σ Planck constraints for models with variable n_s , $dn_s/d \ln k$ and r , obtained from the Planck Legacy Archive. The star corresponds to the reference parameter choice $(x_c, c) = (0.78, 0.48)$.

Since in this economical model, the inflaton is the Higgs of the Standard Model, the connection with particle physics is direct, and we can derive the couplings of the model, which will depend on the concrete parameter choice. For instance, we show in color in Fig. 5 the values of the non-minimal coupling ξ at CMB scales. For our reference values, we find that $\lambda_0 = 1.195 \times 10^{-6}$, $\xi_0 = 21$, $\kappa^2 \mu^2 = 0.0226$, $b_\lambda = 0.9 \times 10^{-5}$ and $b_\xi = 40.6$. These values are consistent, within 2σ , with the measured Higgs parameters at the LHC. Future measurements of the PBH mass spectrum will allow us to determine the SM couplings of the Higgs and their RGE running from the EW

scale to almost the Planck scale. A detailed analysis of the compatibility of these coefficients with the predictions of the SM non-minimally coupled to gravity requires further work (in progress).

It is also interesting to note that this CHI scenario predicts an amplitude of tensor modes that lies within the target range of present and next-generation B-mode experiments [35]. Moreover, the large amplitude of curvature fluctuations a few e -folds before the end of inflation, see Fig. 4, may induce a significantly inhomogeneous reheating upon reentry, which could have important consequences for the reheating temperature and possibly also for the production of PBH and gravitational waves at preheating, see e.g. [36]. In particular, we find that the energy density at the end of inflation is $\rho_{\text{end}} = 2.8 \times 10^{63} \text{ GeV}^4$ and the estimated reheating temperature (for $g_* = 106.75$), $T_{\text{rh}} = 3 \times 10^{15} \text{ GeV}$, is relatively high.

(a) Production of PBHs and DM

We use the Press-Schechter formalism of gravitational collapse to compute the probability that a given horizon-sized volume forms a PBH when a large curvature fluctuation reenters the horizon during the radiation era, and not even radiation pressure can prevent collapse [37]. The mass of the PBH at formation is essentially given by the mass within the horizon at the time of reentry. In our case, for the large, flat and wide peak in $\mathcal{P}_{\mathcal{R}}(k)$ at small scales, see Fig. 4, one finds a lognormal distribution of masses for PBH,

$$P(M) = \frac{A \mu}{M \sqrt{2\pi\sigma^2}} \exp\left(-\frac{\ln^2(M/\mu)}{2\sigma^2}\right).$$

The distribution of PBHs at equality is fully characterized by the physics of inflation, its evolution during radiation domination and the evaporation due to Hawking radiation. We find that for the chosen parameters PBHs constitute the total DM at equality, i.e. $\Omega_{\text{PBH}}^{\text{eq}} = 0.42$.

From equality to present times, the mass distribution will shift to higher masses due to merging and accretion. In this CHI scenario, there is a very wide and flat peak in the matter spectrum at small scales. This means that PBHs will cluster in very dense environments, which can significantly increase the frequency of black-hole-binary mergers. In order to exactly determine the mass distribution of PBHs today, one would have to solve the non-linear evolution with a N-body simulation. Following Ref. [38], we estimate the growth in PBH masses by a factor $\sim 10^{20}$, although it could be significantly larger. In this case, we find that the mean of the lognormal distribution corresponds today to approximately $\mu_{\text{PBH}} \simeq 10 M_{\odot}$ and the lognormal dispersion to $\sigma_{\text{PBH}} \simeq 1.4$. Therefore, Dark Matter is dominated today by PBH with masses in the range from 10^{-2} to $10^3 M_{\odot}$, between the size of large planets and intermediate mass black holes. This range of PBH produced in the CHI scenario passes all observational constraints without difficulty, see Fig. 6. The fact that the scenario predicts a very wide mass range helps, since it can achieve $\Omega_{\text{DM}} = \Omega_{\text{PBH}}$ in an integrated way, without having to saturate the bound at any given mass scale. Moreover, the microlensing constraints are significantly weakened since PBH strongly cluster in this model [27]. On the other hand, these PBH are difficult to detect with FermiLAT via femtolensing of GRB [39]. Even with microlensing experiments of distant QSO it is going to be a challenge [40].

5. Conclusion

We have explored the possibility that the Standard Model Higgs, with a non-minimal coupling to gravity, may have acted as the inflaton in the early universe, and produced all of the present dark matter from quantum fluctuations that reentered the horizon as huge curvature perturbations and collapsed to form black holes much before primordial nucleosynthesis. Taking into account the RGE running of both the Higgs self-coupling λ and the non-minimal coupling to gravity ξ , we find regions of parameter space allowed by the Standard Model for which the inflaton-Higgs potential acquires a second plateau at smaller scales, around the critical point $\lambda(\mu) \simeq \beta_{\lambda}(\mu) = 0$. This plateau gives a super-slow-roll evolution of the Higgs, inducing a high peak in the curvature

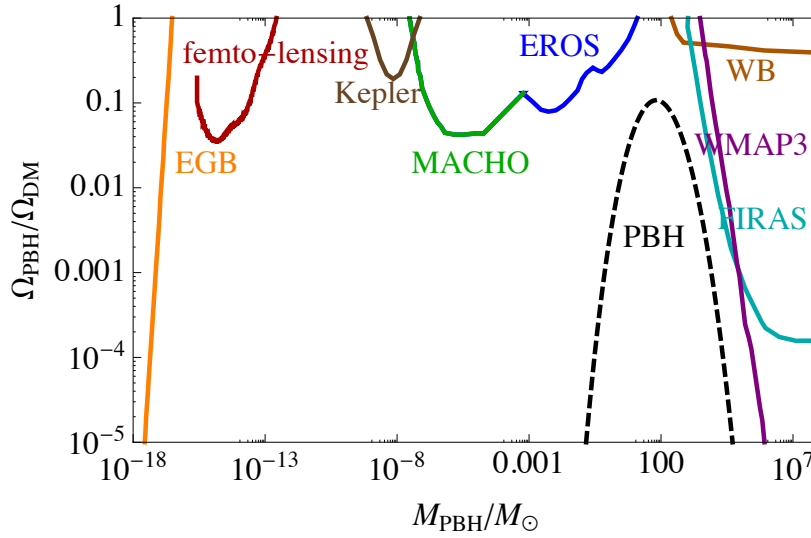


Figure 6. Present constraints on PBH from Extragalactic Gamma Background (EGB), femto-lensing of GRB, micro-lensing (Kepler, MACHO and EROS), Wide Binaries (WB) and the CMB (FIRAS and WMAP3). The massive primordial black holes (dashed-dotted line) produced in Critical Higgs Inflation could comprise all of the dark matter and still pass all the constraints. See Refs. [43,44] for a review.

power spectrum which is almost flat and very broad, lasting for many e -folds. When those fluctuations reenter the horizon during the radiation era they collapse to form primordial black holes with very small masses, which grow via accretion and merging, into the mass range 10^{-2} to $10^3 M_{\odot}$, evading all of the present constraints on PBH [43,44], thanks to their strong clustering. Some of these PBH may evaporate before equality; the rest will act as seeds for galactic structures [27] and initiate reionization at high redshift [45]. Such a high peak in the matter power spectrum occurs at so small scales that there are no significant constraints coming from large scale structures. This scenario of massive PBH could explain the missing satellite problem, as well as the large mass-to-light ratios found in dwarf spheroidals [27,46], and is not in conflict with Fermi-LAT gamma-ray observations [47]. A possible direct detection could come from microlensing events by Kepler on distant QSO [40]. Alternatively, the stochastic background of gravitational waves from the merging of black hole binaries in the dense clusters after equality could be detectable by LISA or PTA [41,42]. Moreover, this CHI scenario has also distinctive inflationary signatures, such as large fluctuations at the end of inflation that may lead to a phase of inhomogeneous reheating.

But, more importantly, the PBH-CHI scenario opens a new portal to test fundamental physics above the LHC scale. The RGE running of the SM Higgs couplings, from the electroweak scale to almost the Planck scale, may contribute to our understanding of the stability of the electroweak vacuum and, moreover, to constrain new physics beyond the Standard Model of Particle Physics.

Competing Interests. The author declares that he has no competing interests.

Funding. This work is supported by the Research Project FPA2015-68048-03-3P [MINECO-FEDER], and the Centro de Excelencia Severo Ochoa Program SEV-2012-0249.

Acknowledgements. I thank Savvas Nesseris, Manuel Trashorras, José María Ezquiaga and Ester Ruiz Morales for fruitful discussions. This proceeding is based on work done in collaboration with them.

References

1. M. Shaposhnikov and D. Zenhausern, *Phys. Lett. B* **671**, 187 (2009)
2. J. García-Bellido, J. Rubio, M. Shaposhnikov and D. Zenhausern, *Phys. Rev. D* **84**, 123504 (2011)
3. J. García-Bellido, J. Rubio and M. Shaposhnikov, *Phys. Lett. B* **718**, 507 (2012)

4. F. L. Bezrukov and M. Shaposhnikov, *Phys. Lett. B* **659**, 703 (2008)
5. J. García-Bellido, D. G. Figueroa and J. Rubio, *Phys. Rev. D* **79**, 063531 (2009)
6. P. A. R. Ade *et al.* [Planck Collaboration], *Astron. Astrophys.* **594**, A13 (2016)
7. P. Bull *et al.*, *Phys. Dark Univ.* **12**, 56 (2016)
8. M. Trashorras, S. Nesseris and J. García-Bellido, *Phys. Rev. D* **94**, 063511 (2016)
9. K. Nakamura *et al.* [Particle Data Group], *J. Phys. G* **37**, 075021 (2010)
10. D. Blas, M. Shaposhnikov and D. Zenhausern, *Phys. Rev. D* **84**, 044001 (2011)
11. D. Buttazzo, G. Degrassi, P. P. Giardino, G. F. Giudice, F. Sala, A. Salvio and A. Strumia, *JHEP* **1312**, 089 (2013)
12. C. D. Froggatt and H. B. Nielsen, *Nucl. Phys. B* **147**, 277 (1979)
13. J. García-Bellido and D. Wands, *Phys. Rev. D* **53**, 5437 (1996)
14. D. H. Lyth, "Introduction to Cosmology," *astro-ph/9312022*.
15. P. A. R. Ade *et al.* [Planck Collaboration], *Astron. Astrophys.* **571**, A22 (2014)
16. V. F. Mukhanov, H. A. Feldman and R. H. Brandenberger, *Phys. Rept.* **215**, 203 (1992)
17. J. M. Bardeen, *Phys. Rev. D* **22**, 1882 (1980)
18. H. Kodama and M. Sasaki, *Prog. Theor. Phys. Suppl.* **78**, 1 (1984)
19. J. García-Bellido and D. Wands, *Phys. Rev. D* **52**, 6739 (1995)
20. G. Pantazis, S. Nesseris and L. Perivolaropoulos, *Phys. Rev. D* **93**, no. 10, 103503 (2016)
21. E. J. Copeland, A. R. Liddle and D. Wands, *Phys. Rev. D* **57**, 4686 (1998)
22. P. G. Ferreira and M. Joyce, *Phys. Rev. D* **58**, 023503 (1998)
23. R. J. Scherrer and A. A. Sen, *Phys. Rev. D* **77**, 083515 (2008)
24. B. P. Abbott *et al.*, *Phys. Rev. Lett.* **116**, 061102 (2016).
25. S. Bird *et al.*, *Phys. Rev. Lett.* **116**, 201301 (2016); S. Clesse and J. García-Bellido, *Phys. Dark Univ.* **10**, 002 (2016); M. Sasaki *et al.*, *Phys. Rev. Lett.* **117**, 061101 (2016).
26. J. García-Bellido, A. D. Linde and D. Wands, *Phys. Rev. D* **54**, 6040 (1996).
27. S. Clesse & J. García-Bellido, *Phys. Rev. D* **92**, 023524 (2015).
28. J. García-Bellido and E. Ruiz Morales, "Primordial black holes from single-field models of inflation," *arXiv:1702.03901*, to appear in JCAP.
29. J. M. Ezquiaga, J. García-Bellido and E. Ruiz Morales, "Primordial Black Hole production in Critical Higgs Inflation," *arXiv:1705.04861*.
30. P. A. R. Ade *et al.* [Planck Collaboration], *Astron. Astrophys.* **594**, A20 (2016)
31. F. L. Bezrukov and M. Shaposhnikov, *Phys. Lett. B* **659**, 703 (2008).
32. J. García-Bellido, D. G. Figueroa and J. Rubio, *Phys. Rev. D* **79**, 063531 (2009).
33. F. Bezrukov and M. Shaposhnikov, *Phys. Lett. B* **734**, 249 (2014);
Y. Hamada, H. Kawai, K. y. Oda and S. C. Park, *Phys. Rev. Lett.* **112**, 241301 (2014).
34. M. Herranen, T. Markkanen, S. Nurmi and A. Rajantie, *Phys. Rev. Lett.* **115**, 241301 (2015).
35. BICEP/Keck Collaboration <http://bicepkeck.org/>;
ACT Collaboration <http://act.princeton.edu/>;
Simons Array Collaboration <http://simonsobservatory.org/>;
LiteBird Collaboration <http://litebird.jp/>.
36. J. García-Bellido and D. G. Figueroa, *Phys. Rev. Lett.* **98**, 061302 (2007).
37. T. Harada, C. M. Yoo and K. Kohri, *Phys. Rev. D* **88**, 084051 (2013).
38. J. R. Chisholm, *Phys. Rev. D* **73**, 083504 (2006).
39. A. Barnacka, J. F. Glicenstein and R. Moderski, *Phys. Rev. D* **86**, 043001 (2012).
40. K. Griest, M. J. Lehner, A. M. Cieplak and B. Jain, *Phys. Rev. Lett.* **107**, 231101 (2011).
41. S. Clesse and J. García-Bellido, "Detecting the gravitational wave background from primordial black hole dark matter," *arXiv:1610.08479* [*astro-ph.CO*].
42. N. Bartolo *et al.*, *JCAP* **1612**, 026 (2016).
43. J. García-Bellido, "Massive Primordial Black Holes as Dark Matter and their detection with Gravitational Waves," *arXiv:1702.08275*, to appear in the Proceedings of the XIth LISA Symposium, Zürich (2016).
44. B. Carr, F. Kuhnel and M. Sandstad, *Phys. Rev. D* **94**, 083504 (2016).
45. A. Kashlinsky, *Astrophys. J.* **823**, L25 (2016).
46. T. S. Li *et al.* [DES Collaboration], *Astrophys. J.* **838**, 8 (2017).
47. R. Bartels *et al.*, *Phys. Rev. Lett.* **116**, 051102 (2016);
S. K. Lee *et al.*, *Phys. Rev. Lett.* **116**, 051103 (2016).